Physics of Fluids

LETTER | APRIL 01 2025

Bubble-bearing fluid flows on an inclined plane

Kohei Ohie (大家広平); Yuji Tasaka (田坂裕司); Yuichi Murai (村井祐一)

Physics of Fluids 37, 041701 (2025)
https://doi.org/10.1063/5.0261398

Physics of Fluids LETTER pubs.aip.org/aip/pof

Bubble-bearing fluid flows on an inclined plane

Cite as: Phys. Fluids **37**, 041701 (2025); doi: 10.1063/5.0261398
Submitted: 30 January 2025 · Accepted: 13 March 2025 ·
Published Online: 1 April 2025

View Online Export Citation CrossMark

Kohei Ohie (大家広平),[1,a] Yuji Tasaka (田坂裕司),[1,2] and Yuichi Murai (村井祐一)[1]

AFFILIATIONS

[1]Laboratory for Flow Control, Faculty of Engineering, Hokkaido University, Sapporo, Japan
[2]Research Institute for Marine Geodynamics, Japan Agency for Marine-Earth Science and Technology, Yokosuka, Japan

[a)]Author to whom correspondence should be addressed: ohie@eis.hokudai.ac.jp

ABSTRACT

The effect of bubble-bearing state on fluid flows on an inclined plane is clarified. The deceleration or acceleration compared to the single-phase state is determined by a non-dimensional parameter Π, a ratio of the gravity-induced shear stress to the restoring force originated by the surface tension. At $\Pi < O(1)$, the spherical bubbles contribute to increasing the viscosity and decelerating the flow. At $\Pi > O(1)$, the deformed bubbles decrease the viscosity and accelerate the flow. The result is validated in experiments under the former condition, and this framework is applied to predict the arrival time of the bubble-bearing fluid flows. Through this work, it is shown that extending the application of the rheology model beyond just materials science to fluid mechanics offers new avenues for elucidating the underlying physics of bubble-bearing fluid flows across diverse disciplines.

Bubble-bearing fluid flows on an inclined plane are commonly observed in nature, such as lava and mud flows,[1] as well as in the manufacturing processes of the paper, glass, concrete, and steel industries. Studies on these flows have a broad impact on both hazard assessment and product quality enhancement. The bubble-bearing state lowers the effective density of the fluid; meanwhile, it modifies the bulk rheological properties compared to the single-phase state.[2–4] The competition between these opposing effects makes it not straightforward whether the dispersed bubbles contribute to accelerating or decelerating the flows.[5,6]

Studies on bubble suspension rheology have a century-long history originated by Einstein[7] and Taylor.[8] Through rigorous theoretical work by Frankel and Acrivos[9] and subsequent experimental work,[10–20] the rheology under steady shear is well rationalized by

$$\eta_r = 1 + \frac{1 - 12Ca^2/5}{1 + (6Ca/5)^2}\phi. \tag{1}$$

The relative viscosity η_r is the effective viscosity of the suspension normalized by that of the continuous phase. The capillary number Ca is a non-dimensional parameter defined as $Ca = \lambda\dot{\gamma}$ with the relaxation time of the suspended bubble λ and shear rate $\dot{\gamma}$ applied to the suspension. This formula is experimentally validated by Morini *et al.*[17] at the volume fraction of $\phi < 20\%$ and $Ca < 10$. When Ca is lower than the critical value, $Ca_c = 0.65$, the viscosity increases as ϕ increases while the viscosity decreases at $Ca > Ca_c$.

Llewellin *et al.*[12] further investigated the viscoelastic properties of dilute bubble suspensions when a small amplitude oscillatory shear is applied. They semi-empirically derived that the deviatoric stress tensor $\boldsymbol{S}$ and shear rate tensor $\dot{\boldsymbol{\gamma}}$ are related as

$$\boldsymbol{S} + \frac{6}{5}\lambda\frac{d\boldsymbol{S}}{dt} = \mu_0(1+\phi)\dot{\boldsymbol{\gamma}} + \frac{6}{5}\mu_0\lambda\left(1 - \frac{5}{3}\phi\right)\frac{d\dot{\boldsymbol{\gamma}}}{dt}. \tag{2}$$

The shear rate tensor is defined as $\dot{\boldsymbol{\gamma}} = 2\boldsymbol{d}$ with the rate of deformation tensor $\boldsymbol{d} = [\nabla\boldsymbol{u} + (\nabla\boldsymbol{u})^T]/2$ and the velocity of the suspension $\boldsymbol{u}$, where the velocity gradient tensor is defined as $(\nabla\boldsymbol{u})_{ij} = \partial u_i/\partial x_j$. Mitrias *et al.*[21] validated the above-mentioned constitutive equation by direct numerical simulation, and Mitrou *et al.*[20] recently investigated the effects of bubble size polydispersity on the linear viscoelastic behavior. Mader *et al.*[22] further took a theoretical approach to establish a more comprehensive constitutive equation covering both Eqs. (1) and (2) based on the constitutive equation originally proposed by Frankel and Acrivos.[9] They showed that the viscoelastic property is systematized by Ca and dynamic capillary number Cd, which represents the unsteadiness of the bubble deformation. Ohie *et al.*[19] presented rheology mapping[23] that comprehensively expresses the dependence of the relative viscosity and the phase of viscoelasticity on both Ca and Cd, and not only experimentally verified it but also provided a holistic picture of bubble suspension rheology. Among these rheological models, which also include an equation accounting for unsteady flows, Eq. (1) is primarily used in this study, as it focuses on the steady flows of bubble suspensions here.

The bubble suspension rheology is in its mature stage, and the reliable model can now be applied to unravel the physics of complex bubble-bearing fluid flows. Now, we consider a flow on an inclined plane as shown in Fig. 1, which is fundamental but widely observed as described above.[24] Mono-disperse bubbles are uniformly distributed in a Newtonian fluid, and the suspension is flowing on the plane of an angle θ. The flow is assumed to be two dimensional (uniform in the spanwise direction) and non-slip at $y = 0$. The thickness of the fluid layer is h and it is a free surface at $y = h$. In the case of a Newtonian fluid ($\phi = 0\%$), the flow rate is

$$Q_0 = \frac{\rho_0 g h^3 \sin\theta}{3\mu_0}, \tag{3}$$

with the density ρ_0, gravitational acceleration g, and viscosity coefficient μ_0. In the derivation of the above-mentioned equation, it is also assumed that the flow is laminar, unidirectional, and that the liquid thickness is constant. Although there are multiple parameters involved, the effects of the density reduction and the rheological modification on the flow may be governed in terms of ϕ and Ca. In this Letter, we clarify the effect of bubble-bearing state on the flow. Based on the momentum balance equation and the rheology model, the velocity distribution is theoretically derived first. Non-dimensionalization of the equation unveils two non-dimensional parameters to characterize the flow. Experimental validation is given accordingly, and some application examples are demonstrated. Concluding remarks are finally given.

Now, consider a situation in which a bubble suspension with a continuous phase density ρ_0 and volume fraction ϕ flows down an inclined plane, as shown in Fig. 1. The flow of the bubble suspension in bulk is considered, that is, the flow is assumed as a continuous non-Newtonian fluid flow with effective density $\rho_0(1-\phi)$ and the constitutive equation is given by Eq. (1). A suspension can be generally regarded as a continuum when the characteristic length scale of the flow is at least an order of magnitude larger than the suspended phase.[25–27] It is, therefore, assumed here that the thickness of the fluid layer is sufficiently larger than the bubble size. We start with the Cauchy momentum equation for the suspension, which describes the relationship between the velocity vector $\boldsymbol{u}$, the stress tensor $\boldsymbol{\sigma}$, and the body force vector $\boldsymbol{b}$ as

$$\rho_0 \frac{D\boldsymbol{u}}{Dt} = \nabla \cdot \boldsymbol{\sigma} + \rho_0 \boldsymbol{b}, \tag{4}$$

where the operator D/Dt is Lagrangian derivative. Assuming a Cartesian coordinate system fixed on an inclined plane, as shown in

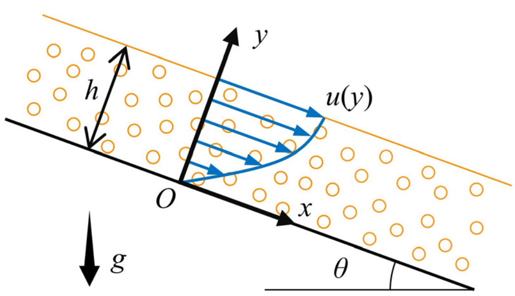

FIG. 1. Schematic of the bubble-bearing fluid flow on an inclined plane.

Fig. 1, and steady unidirectional flow, the shear stress profile $\tau = \sigma_{xy}$ is given as[28]

$$\tau = \rho_0(1-\phi) g \sin\theta (h - y). \tag{5}$$

The stress takes the maximum value, $\rho_0(1-\phi)gh\sin\theta$, at $y = 0$ and linearly decreases toward the free surface at $y = h$. The stress is also given as $\tau = \eta_r \mu_0 \dot{\gamma}$ with $\dot{\gamma} = du/dy$ and Eq. (1). Therefore, Eq. (5) is modified to

$$\mu_0 \left(1 + \frac{1 - 12\lambda^2\dot{\gamma}^2/5}{1 + (6\lambda\dot{\gamma}/5)^2} \phi \right) \dot{\gamma} = \rho_0(1-\phi) g \sin\theta (h - y). \tag{6}$$

When the volume fraction is $\phi = 0\%$, that is, a Newtonian fluid single-phase case, the velocity distribution is given as

$$u(y) = \frac{\rho_0 g \sin\theta}{2\mu_0} y(2h - y), \tag{7}$$

and the flow rate per unit length in the direction of x axis, Q_0, is given as Eq. (3). In the case of a bubble suspension ($\phi > 0\%$), Eq. (6) is a cubic equation of $\dot{\gamma}$, the real solution is obtained by Cardano's formula at each y. The profile $\dot{\gamma}(y)$ is thus obtained and the velocity $u(y)$ is also obtained by integrating $\dot{\gamma}(y)$ with a non-slip condition at $y = 0$.

The velocity profiles under two different θ are exemplarily shown in Fig. 2. The volume fraction is $\phi = 20\%$, and the other parameters are tentatively set as $\rho_0 = 1000\,\mathrm{kg/m^3}$, $g = 9.81\,\mathrm{m/s^2}$, $h = 0.05\,\mathrm{m}$, $\mu_0 = 10\,\mathrm{Pa \cdot s}$, and $\lambda = 0.2\,\mathrm{s}$. At $\theta = 5\,\mathrm{deg}$, the addition of the bubbles contributes to the deceleration of the flow compared to the single-phase state, in contrast, it contributes to the acceleration of the flow at $\theta = 20\,\mathrm{deg}$. The dashed lines in the graphs show $Ca = Ca_c$. Above this critical line ($Ca < Ca_c$), the bubbles maintain a spherical shape and the effective viscosity increases. In contrast, for $Ca > Ca_c$, the bubbles are deformed and contribute to a decrease in the viscosity. The driving force increases by inclining the plane, and hence the region of the viscosity reduction enlarges and the flow totally accelerates as θ increases.

The results in Fig. 2 are under the specific parameters set tentatively. Non-dimensionalization of Eq. (6) is conducted here to identify the governing parameters. With representative time scale λ and length scale h, the shear rate and height are reduced as $\dot{\gamma}^* = \lambda\dot{\gamma}$ and $y^* = y/h$, where the asterisk indicates a non-dimensional variable. Substituting these into Eq. (6), we obtain

$$\left(1 + \frac{1 - 12\dot{\gamma}^{*2}/5}{1 - (6\dot{\gamma}^*/5)^2} \phi \right) \dot{\gamma}^* = \Pi(1-\phi)(1 - y^*). \tag{8}$$

The parameter Π is defined as

$$\Pi = \frac{\rho_0 g h \sin\theta}{\mu_0/\lambda} = \frac{\rho_0 g h \sin\theta}{\sigma/a}. \tag{9}$$

The flow is, therefore, systematized with Π and ϕ. The relaxation time is given by $\lambda = \mu_0 a/\sigma$ with the bubble radius a and the surface tension σ.[11,12] The numerator on the far right in Eq. (9) represents the gravity-induced shear stress in the single-phase state, and the denominator restores the pressure originated by the surface tension. A similar parameter was proposed by Namiki *et al.*[6] by roughly estimating the shear rate in the suspension layer.

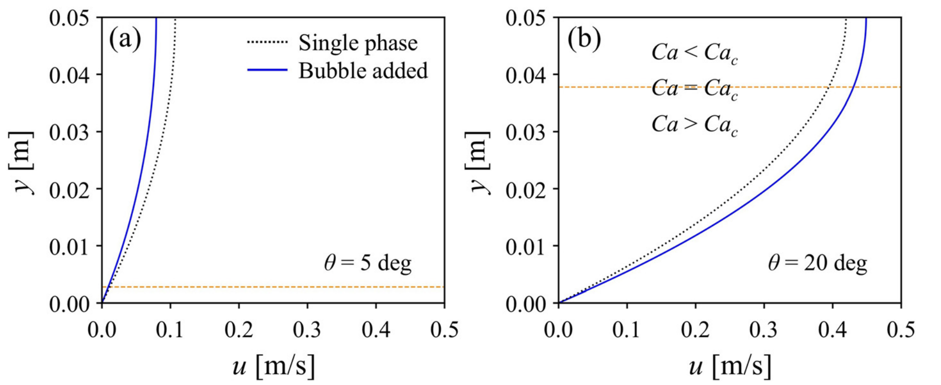

FIG. 2. Velocity profiles of the bubble-bearing fluid at different angles of (a) $\theta = 5$ deg and (b) $\theta = 20^{\circ}$. The dotted curves are at $\phi = 0\%$ for comparison. The dashed lines are at where the capillary number Ca takes the critical value $Ca_c = 0.65$.

Solving Eq. (8) at each y^* by Cardano's formula, $\dot{\gamma}^*(y^*)$ is obtained. The integral operation on it with a non-slip condition at $y^* = 0$ gives the velocity distribution, $u^*(y^*)$. Further integrating u^* in $0 \leq y^* \leq 1$, the flow rate $Q^*(\Pi, \phi)$ is obtained. The flow rate in the single-phase state is denoted as $Q_0^* = Q^*(\Pi, \phi = 0\%)$. The ratio Q^*/Q_0^* is calculated under different conditions of Π and ϕ [Fig. 3(a)]. It is clear from the comprehensive map that the bubble-bearing state slows down or accelerates the flow depending on whether Π exceeds the critical value, $O(1)$.

When Π is smaller than $O(1)$, the contour lines of Q^*/Q_0^* distribute horizontally, that is, the flow rate ratio only depends on ϕ as shown with blue symbols in Fig. 3(b). In this condition, the bubbles maintain a spherical shape throughout the suspension layer. At $Ca \ll 1$, the relative viscosity is given as $\eta_r = 1 + \phi$ from Eq. (1), which is known as Taylor's formula.[8] The flow rate under this condition is $Q = \rho_0(1-\phi)g\sin\theta h^3/3\mu_0(1+\phi)$. The flow rate ratio is, therefore,

$$\frac{Q^*}{Q_0^*}(\Pi < O(1), \phi) = \frac{1-\phi}{1+\phi}, \tag{10}$$

as shown in the lower solid line in Fig. 3(b), which well fits the symbols at $\Pi = 10^{-1}$. In contrast, when Π is larger than $O(1)$, the bubbles are deformed throughout the suspension layer. At $Ca \gg 1$, the relative viscosity is given as $\eta_r = 1 - 5\phi/3$ from Eq. (1).[29] The flow rate in this condition is $Q = \rho_0(1-\phi)g\sin\theta h^3/3\mu_0(1-5\phi/3)$. The flow rate ratio is, therefore,

$$\frac{Q^*}{Q_0^*}(\Pi > O(1), \phi) = \frac{1-\phi}{1-5\phi/3}, \tag{11}$$

as shown with the upper solid line in Fig. 3(b), which also well fits the red symbols. In summary, the deceleration or acceleration is determined by Π. The flow ratio follows Eq. (10) at $\Pi < O(1)$ and Eq. (11) at $\Pi > O(1)$. It should be noted that the map representation shown in Fig. 3(a) quantifies the degree of acceleration or deceleration not only in the extreme cases of Π but also near unity, giving a holistic picture of bubble-bearing fluid flows on an inclined plane.

As validation of the theoretical work, laboratory scale experiments were conducted. An acrylic plate was fixed with an inclined angle of $\theta = 30$ deg. A portion of liquid was poured from the top, and the creeping flow was captured by a camera (Fig. 4). The continuous

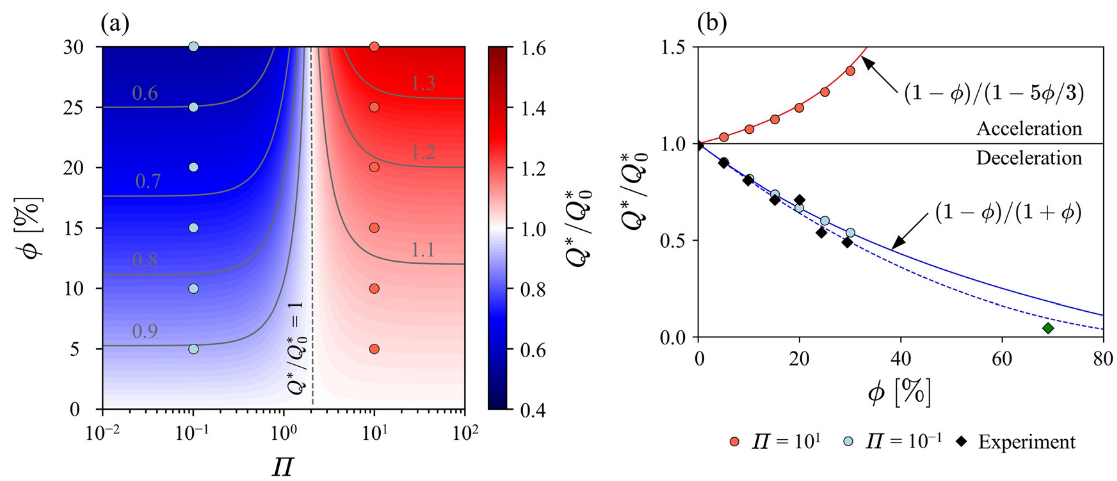

FIG. 3. (a) Flow rate ratio under different Π and volume fraction ϕ, and (b) dependence of the flow rate ratio at $\Pi = 10^{-1}$ and $\Pi = 10^1$. The diamond symbols represent the experimental results at $\Pi = O(10^{-1})$. The green symbol at $\phi = 69\%$ is the flow rate ratio evaluated from the data in the previous model experiment conducted by Namiki *et al.*.[6]

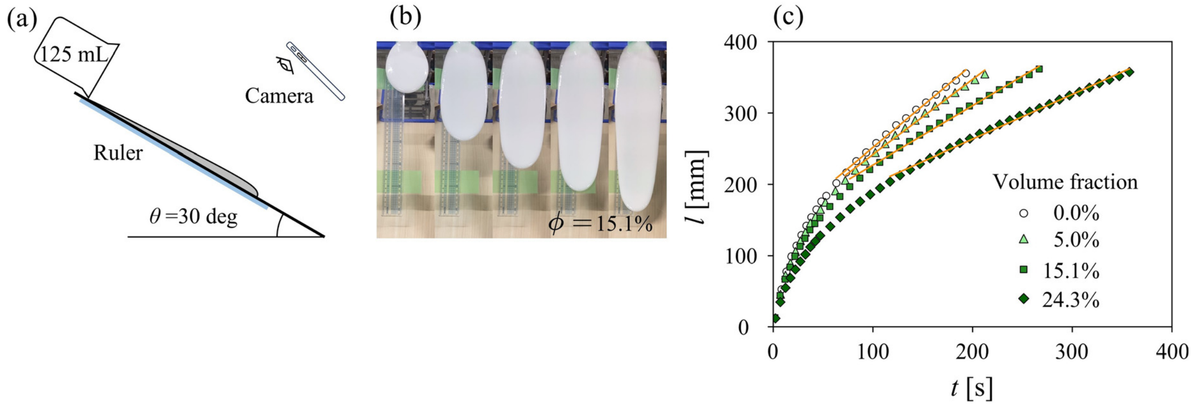

FIG. 4. (a) Schematic of the experimental setup, (b) a series of photos taken from the top every minute, and (c) time variations of the tip positions of the bubble-bearing fluids moving down the slope under different volume fractions. The orange solid lines are linear regression results in the range of $l \geq 200$ mm.

phase is starch syrup ($\rho_0 = 1400\,\mathrm{kg/m^3}$, $\sigma = 0.07\,\mathrm{N/m}$), which is Newtonian. The bubbles were generated by the chemical reaction of citric acid and baking soda. Bubble suspensions with various volume fractions can be prepared by changing the reaction time. The suspensions were prepared with volume fractions ranging from approximately 5% to 30%. Specifically, a beaker was filled with starch syrup, to which citric acid and baking soda, finely ground using a mortar, were added. These were manually mixed using a spatula. The total volumes immediately after mixing and that after a certain period, following the completion of the foaming process, were measured using the graduated markings on the beaker. The bubble volume fraction was then estimated based on these volumes. The generated bubble size was confirmed to be $O(0.1)$ mm and the thickness of the suspension layer is $O(1)$ mm. The bubble radius distribution at a volume fraction of approximately 20% is shown in the histogram in Fig. 5. The viscosity of the continuous phase is $O(10)$ Pa · s, the bubble rise velocity in the continuous phase is, therefore, estimated to be $O(10^{-7})$ m/s. Given that the vertical displacement during the following experiments is only $O(10^{-2})$ mm, the stability of the bubble-bearing state is fully assured. The generated bubble size is likely to be polydisperse, as shown in

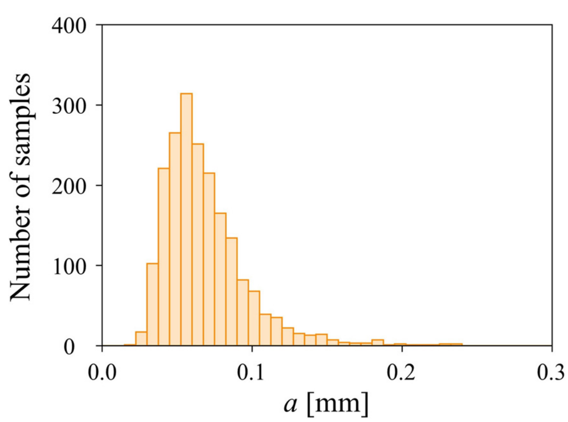

FIG. 5. Histogram of the bubble radius distribution at a volume fraction of approximately 20%.

Fig. 5, but it has been demonstrated by Mitrou *et al.*[18] that Eq. (1) remains valid in such cases. In these conditions, $\Pi = O(10^{-1})$, the bubbles are expected to decelerate the flow according to the condition discussed above.

Time variations of the tip positions are summarized in Fig. 4(c) for representative volume fractions. As expected, the flow slows down as ϕ increases. The creeping velocity is determined by linear fitting in the range of $l > 200$ mm, where the pouring has finished and the gradient is almost constant. The portion of starch syrup and all the suspensions that flowed on the inclined plane with almost the same periphery shape; the velocity ratio of the starch syrup and the suspensions can be interpreted as the flow rate ratios, Q^*/Q_0^*. The results are shown with the diamond symbols in Fig. 3(b). The experimental results are arranged on the line of $Q^*/Q_0^* = (1-\phi)/(1+\phi)$. The experiments were conducted in the condition of $\Pi = O(10^{-1})$, this is, therefore, reasonable and reinforces the above-mentioned theoretical work. Despite being a very simple experiment, it reflects the shear viscosity of bubble-bearing fluids validly.

A similar model experiment was previously conducted by Namiki *et al.*[6] on a larger scale. The experiment was also in the condition of $\Pi < O(1)$, but with a more higher volume fraction at $\phi = 69\%$. Based on their data regarding the time evolution of the creeping flow length, the flow rate ratio was evaluated,[30] shown with a green diamond symbol in Fig. 3(b). Although the bubble-bearing fluid at the volume fraction is like a foam[31,32] rather than a suspension state, which is out of the applicable range of Eq. (1), the decelerated flow rate ratio is roughly predicted by the theory. Strictly, it was evaluated lower than the theory. In Eq. (1), the interaction between the bubbles is not considered, but as the volume fraction increases, the interactions between the suspended bubbles are not negligible, and the effective viscosity is evaluated higher than Eq. (1). This is the major reason for the deviation of the experimental data with the theory at $\phi = 69\%$. Several formulas have been proposed to account for higher volume fractions. For example, Llewellin and Manga[5] provided a relationship where the relative viscosity is expressed as $\eta_r = (1-\phi)^{-1}$ at $Ca < Ca_c$. The flow rate under this condition is $Q = \rho_0(1-\phi)^2 g \sin\theta h^3/3\mu_0$. The flow rate ratio is thus given as $Q^*/Q_0^* = (1-\phi)^2$, which is shown as a dashed line in Fig. 3(a). This predictive equation aligns more closely with the experimental values, reaffirming the importance of selecting an appropriate rheology model based on the volume fraction and deformation state of the bubbles. Regarding the limitations of this physical model, when strong shear leads to bubble fragmentation, the resulting decrease in bubble radius reduces Π, which acts to decelerate the flow. Conversely, as the volume fraction further increases and bubbles coalesce due to shear, their radius enlarges, leading to an increase in Π, which contributes to the flow acceleration. Note that these modifications in bubble size over time are not considered in the present physical model.

The primary objective of this study is to apply the rheology model of bubble suspensions to flow predictions. As a fundamental step, the prediction of shear flow on an inclined plane was demonstrated. This theoretical framework is finally applied to the arrival prediction of bubble-bearing fluid flows as an illustrative example. As shown in Figs. 6(a) and 6(b), two geometries are considered, where the first one has a single slope with an angle of $\theta_1 = 30$ deg, and the other consists of two combined slopes with angles of $\theta_2 = 40.9$ deg and $\theta_3 = 16.1$ deg. The height is 100 m and the width is 173 m in both geometries. The lengths of each slope are different, $l_1 = 200$ m and $l_2 + l_3 = 205$ m, where the combined slopes geometry has a longer length by 2.5%. When a bubble-bearing fluid with the same properties that was set in Figs. 2(b) and 2(c) is poured from the top with $Q = 0.01\,\mathrm{m^2/s}$, the questions here are in which geometry the flow approaches the lower end faster and how different they are.

The dependence of the flow rate Q on h is calculated [Fig. 6(c)]. Searching the cross point of each curve with $Q = 0.01\,\mathrm{m^2/s}$, each thickness is determined as $h_1 = 0.038$ m, $h_2 = 0.034$ m, and $h_3 = 0.047$ m. The representative velocity at each slope is obtained as the flow rate divided by each thickness, $u_1 = 0.26\,\mathrm{m/s}$, $u_2 = 0.29\,\mathrm{m/s}$, and $u_3 = 0.21\,\mathrm{m/s}$. The time flowing on each slope is $T_1 = 758$ s and $T_2 + T_3 = 819$ s. The arrival time is, therefore, one minute, that is, 8.0%, slower in the combined slopes geometry although it has longer length only by 2.5%. This result shows that the framework based on the rheology model, rather than just geometric length, is crucial for the accurate prediction of bubble-bearing fluid flows on an inclined plane.

In this Letter, the effect of a bubble-bearing state on a fluid flowing on an inclined plane was investigated. The bubble-bearing state reduces the effective density of the suspension, thereby acting to decelerate the flow. In contrast, bubble suspensions may exhibit either an increase or a decrease in the effective viscosity depending on the deformation state of the bubbles, specifically whether the capillary number exceeds its critical value. To elucidate the effects of changes in density and rheology on the flow, the velocity distribution is theoretically derived from the momentum balance and the bubble suspension rheology model. Based on these equations, it was found that the deceleration or acceleration is determined by a non-dimensional parameter Π [see Eq. (9)], which is the ratio of the gravity-induced shear stress in the single-phase state and the restoring pressure originated by the surface tension. At $\Pi < O(1)$, the deceleration occurs, and the flow rate ratio of the bubble-bearing state against the single-phase state converges to Eq. (10). In the opposite condition, the acceleration occurs, and the flow rate ratio follows Eq. (11). The laboratory scale experiments in the former condition validated the theoretical work. The map representation shown in Fig. 3(a) comprehensively quantifies the degree of acceleration or deceleration not only in these extreme cases of Π but also near unity, providing a holistic picture of bubble-bearing fluid flows on an inclined plane. This fundamental yet essential flow that can be realized even in a kitchen was successfully predicted, indicating that the application of the rheology model beyond just materials science to fluid mechanics will pave the way to unveil the physics of complex bubble-bearing fluid flows in various fields. As many flows in both natural and industrial contexts involve continuous phases with non-Newtonian behaviors, establishing more comprehensive rheological models accounting for this effect and incorporating them into flow predictions will be an important area for future research.

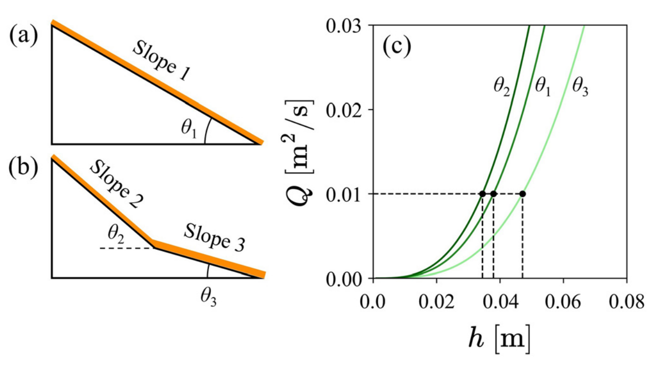

FIG. 6. Arrival time prediction of bubble-bearing fluids: (a) a single slope geometry, (b) combined slopes geometry, and (c) flow rate Q as a function of the suspension layer thickness h under different slope angles.

ACKNOWLEDGMENTS

This work was financially supported by JSPS KAKENHI (Grant No. 22J20991) and the Fukada Geological Institute. The authors would like to thank the reviewers for their constructive comments.

AUTHOR DECLARATIONS

Conflict of Interest

The authors have no conflicts to disclose.

Author Contributions

Kohei Ohie: Conceptualization (equal); Data curation (equal); Formal analysis (equal); Funding acquisition (equal); Investigation (equal); Methodology (equal); Project administration (equal); Resources (equal); Software (equal); Validation (equal); Visualization (equal); Writing – original draft (equal); Writing – review & editing (equal). **Yuji Tasaka:** Conceptualization (equal); Methodology (equal); Project administration (equal); Resources (equal); Supervision (equal); Writing – review & editing (equal). **Yuichi Murai:** Conceptualization (equal); Methodology (equal); Project administration (equal); Resources (equal); Supervision (equal); Writing – review & editing (equal).

DATA AVAILABILITY

The data that support the findings of this study are available from the corresponding author upon reasonable request.

REFERENCES

[1] R. W. Griffiths, "The dynamics of lava flows," Annu. Rev. Fluid Mech. **32**, 477–518 (2000).

[2] H. Pinkerton and R. Sparks, "Field measurements of the rheology of lava," Nature **276**, 383–385 (1978).

[3] A. Harris, S. Mannini, S. Thivet, M. O. Chevrel, L. Gurioli, N. Villeneuve, A. Di Muro, and A. Peltier, "How shear helps lava to flow," Geology **48**, 154–158 (2020).

[4] A. Saiki, K. Yoshimi, K. Nakagawa, Y. Nagasawa, A. Yoshizawa, R. Yanagida, K. Yamaguchi, A. Nakane, K. Maeda, and H. Tohara, "Effects of thickened carbonated cola in older patients with dysphagia," Sci. Rep. **12**, 22151 (2022).

[5] E. W. Llewellin and M. Manga, "Bubble suspension rheology and implications for conduit flow," J. Volcanol. Geotherm. Res. **143**, 205–217 (2005).

[6] A. Namiki, E. Lev, J. Birnbaum, and J. Baur, "An experimental model of unconfined bubbly lava flows: Importance of localized bubble distribution," J. Geophys. Res. Solid Earth **127**(6), e2022JB024139, https://doi.org/10.1029/2022JB024139 (2022).

[7] A. Einstein, "Eine neue bestimung der molekuldimensionen," Ann. Phys. **324**, 289–306 (1906).

[8] G. I. Taylor, "The viscosity of a fluid containing small drops of another fluid," Proc. R. Soc. London A **138**(834), 41–48 (1932).

[9] N. Frankel and A. Acrivos, "The constitutive equation for a dilute emulsion," J. Fluid Mech. **44**, 65–78 (1970).

[10] C. D. Han and R. King, "Measurement of the rheological properties of concentrated emulsions," J. Rheol. **24**, 213–237 (1980).

[11] A. Rust and M. Manga, "Effects of bubble deformation on the viscosity of dilute suspensions," J. Non-Newtonian Fluid Mech. **104**, 53–63 (2002).

[12] E. W. Llewellin, H. M. Mader, and S. D. R. Wilson, "The rheology of a bubbly liquid," Proc. R. Soc. London A **458**(2020), 987–1016 (2002).

[13] R. Pal, "Rheological behavior of bubble-bearing magmas," Earth Planet. Sci. Lett. **207**, 165–179 (2003).

[14] R. Pal, "Rheological constitutive equation for bubbly suspensions," Ind. Eng. Chem. Res. **43**, 5372–5379 (2004).

[15] Y. Murai and H. Oiwa, "Increase of effective viscosity in bubbly liquids from transient bubble deformation," Fluid Dyn. Res. **40**, 565 (2008).

[16] Y. Tasaka, T. Yoshida, R. Rapberger, and Y. Murai, "Linear viscoelastic analysis using frequency-domain algorithm on oscillating circular shear flows for bubble suspensions," Rheol. Acta **57**, 229–240 (2018).

[17] R. Morini, X. Chateau, G. Ovarlez, O. Pitois, and L. Tocquer, "Steady shear viscosity of semi-dilute bubbly suspensions," J. Non-Newtonian Fluid Mech. **264**, 19–24 (2019).

[18] S. Mitrou, S. Migliozzi, P. Angeli, and L. Mazzei, "Effect of polydispersity and bubble clustering on the steady shear viscosity of semidilute bubble suspensions in newtonian media," J. Rheol. **67**, 635–646 (2023).

[19] K. Ohie, Y. Tasaka, and Y. Murai, "Rheology of dilute bubble suspensions in unsteady shear flows," J. Fluid Mech. **983**, A39 (2024).

[20] S. Mitrou, S. Migliozzi, L. Mazzei, and P. Angeli, "On the linear viscoelastic behavior of semidilute polydisperse bubble suspensions in newtonian media," J. Rheol. **68**, 539–552 (2024).

[21] C. Mitrias, N. O. Jaensson, M. A. Hulsen, and P. D. Anderson, "Direct numerical simulation of a bubble suspension in small amplitude oscillatory shear flow," Rheol. Acta **56**, 555–565 (2017).

[22] H. Mader, E. Llewellin, and S. Mueller, "The rheology of two-phase magmas: A review and analysis," J. Volcanol. Geotherm. Res. **257**, 135–158 (2013).

[23] K. Ohie, T. Yoshida, Y. Tasaka, and Y. Murai, "Effective rheology mapping for characterizing polymer solutions utilizing ultrasonic spinning rheometry," Exp. Fluids **63**, 40 (2022).

[24] H. E. Huppert, "Flow and instability of a viscous current down a slope," Nature **300**, 427–429 (1982).

[25] H. A. Barnes, "A review of the slip (wall depletion) of polymer solutions, emulsions and particle suspensions in viscometers: Its cause, character, and cure," J. Non-Newtonian Fluid Mech. **56**, 221–251 (1995).

[26] H. A. Barnes, "Measuring the viscosity of large-particle (and flocculated) suspensions—a note on the necessary gap size of rotational viscometers," J. Non-Newtonian Fluid Mech. **94**, 213–217 (2000).

[27] K. Ohie, D. Nishizuka, T. Yoshida, and Y. Tasaka, "Cost-effective production of density-controllable monodisperse spheres for experiments in fluids," Phys. Fluids **36**, 091704 (2024).

[28] M. O. Deville, *An Introduction to the Mechanics of Incompressible Fluids* (Springer Nature, 2022).

[29] J. Mackenzie, "The elastic constants of a solid containing spherical holes," Proc. Phys. Soc. London Sect. B **63**, 2 (1950).

[30] The descending velocities of the single-phase and bubble-bearing states were evaluated from Figure 5a in the paper by Namiki et al.[6] The velocities at $l > 0.4$ m were roughly evaluated by calculating the gradient of two points at $l = 0.4$ m and 1.2 m. The corresponding velocities are 0.142 m/s and 0.006 m/s for the single-phase and bubble-bearing states, respectively.

[31] S. Besson, G. Debregeas, S. Cohen-Addad, and R. Höhler, "Dissipation in a sheared foam: From bubble adhesion to foam rheology," Phys. Rev. Lett. **101**, 214504 (2008).

[32] J.-C. Géminard, J. Pastenes, and F. Melo, "Foam rheology at large deformation," Phys. Rev. E **97**, 042601 (2018).